scientific reports

Check for updates

OPEN

The RNA-binding protein LARP6 regulates the alternative splicing of related genes in MDA-MB-231 cells

Li Guo[2], Yaobang Liu[2], Shuxun Yan[1], Hong Li[2], Kai Zhang[1] & Jinping Li[2]✉

Triple-negative breast cancer (TNBC) has the highest mortality rate of all breast cancer subtypes and currently lacks effective targeted therapies. LARP6 is an RNA-binding protein associated with cancer promotion, but its mechanism of action in TNBC remains unclear. We conducted RNA sequencing (RNA-seq) and improved RNA immunoprecipitation and sequencing (iRIP-seq) to identify the differentially expressed genes (DEGs) and alternative splice sites bound and regulated by LARP6 in MDA-MB-231 cells. Finally, both RT-qPCR and RIP-qPCR were employed for verification. Our study revealed that LARP6 overexpression altered the expression levels of 171 genes and that the number of regulated alternative splicing events (RASEs) exceeded 1000. The regulated alternative splicing genes (RASGs) corresponding to RASEs were enriched in biological processes such as DNA repair, the cell cycle, and the cellular response to DNA damage stimulus. In addition, we found that LARP6 tends to bind the CGACGAG motif. The intersection of peak-related genes with RASGs suggested that LARP6 can bind to 16 genes and regulate their alternative splicing (AS), thus playing an important role in TNBC progression. Our research indicated that LARP6 may promote the proliferation and invasion of TNBC cells by directly regulating the AS of related genes, providing new clues for targeted therapy for TNBC.

Keywords TNBC, LARP6, Alternative splicing, iRIP-seq, RNA-seq

Triple-negative breast cancer (TNBC) refers to tumours that lack expression of oestrogen receptor (ER), progesterone receptor (PR) and human epidermal growth factor receptor-2 (HER2) according to immunohistochemistry and/or in situ hybridization[1,2]. Epidemiological surveys have revealed that TNBC is highly heterogeneous and clinically aggressive; it accounts for 15–20% of breast cancers, has the highest mortality rate of all breast cancer subtypes, and is common in young premenopausal women[3]. Owing to its unique molecular characteristics, TNBC does not respond well to either endocrine therapy or molecular targeted therapy. As a result, chemotherapy has emerged as the primary systemic treatment. However, the development of drug resistance poses a challenge, as it decreases the efficacy of conventional postoperative adjuvant chemotherapy and radiotherapy. Eventually, residual tumour cell expand, leading to tumour recurrence and metastasis[4,5]. Moreover, there are no targeted therapies for TNBC[6]. Therefore, exploration of the mechanism of invasion and metastasis in TNBC and identification of the molecular target for TNBC treatment are urgently needed.

La ribonucleoprotein domain family member 6 (LARP6) is not only a member of the La ribonucleoprotein family but also an RNA binding protein (RBP). This gene had RNA-binding activity and actively regulates of mRNA-binding activity, translation and subcellular mRNA localization[7,8]. Research into the direct binding targets of LARP6 remains scarce, with the majority of investigations focused on collagen fibres. LARP6 exhibits high specificity in terms of binding affinity for two distinct regions within the 5′-stem-loop structure of both α1(I) and α2(II) collagen mRNAs[9]. This interaction is crucial for regulating the localized translation of these mRNAs, thereby playing a predominant role in the positive regulation of collagen biosynthesis. A study has shown that in TNBC, the expression of LARP6 is strongly upregulated when epithelial–mesenchymal transition (EMT) is induced, and cells undergoing EMT are more dependent on LARP6 for the promotion of protein synthesis to facilitate malignant cell proliferation and invasion[8]. LARP6, an RBP, has been reported to be a key prognostic biomarker in gastric cancer and lung adenocarcinoma[10,11]. These findings suggest that inhibiting LARP6 might be used as a therapeutic target. However, in TNBC, the downstream regulatory targets and underlying regulatory molecular mechanisms of LARP6 remain unclear. Therefore, the function of LARP6 in TNBC needs to be further explored, and its mechanism of action needs to be clarified.

[1]Department of Clinical Medicine, Ningxia Medical University, Yinchuan, China. [2]Department of Surgical Oncology, General Hospital of Ningxia Medical University, No. 804, Shengli Street, Xingqing District, Yinchuan 750001, Ningxia, China. ✉email: 2634497264@qq.com

In this study, we obtained transcriptome data (RNA-seq) data for human breast cancer cells (MDA-MB-231) overexpression LARP6 and then analysed the potential transcriptional and AS targets regulated by LARP6 in MDA-MB-231 cells. Moreover, an LARP6 antibody was used in MDA-MB-231 cells to conduct improved RNA immunoprecipitation combined with high-throughput sequencing (iRIP-seq) to identify the RNA binding targets and motifs of LARP6 in MDA-MB-231 cells. Finally, through integrated analysis of RNA-seq and iRIP-seq data, we found that LARP6 directly binds to multiple genes and promotes TNBC progression mainly by regulating the AS of genes. In conclusion, our study elucidates the LARP6–RNA interaction mechanism in MDA-MB-231 cells, which helps elucidate the regulatory mechanism of LARP6 at the pre-RNA splicing level and provides a basis for an in-depth understanding of the role of LARP6 in various biological processes.

Materials and methods

Cell culture and transfection

The MDA-MB-231 cell line (CL-0150, Procell Life Science & Technology Co., Ltd., China) was cultured at 37 °C with 5% CO_2 in DMEM (PM150210, Procell Life Science & Technology Co., Ltd., China) supplemented with 10% foetal bovine serum (FBS) (10091148, Gibco, China), 100 μg/ml streptomycin, and 100 U/ml penicillin (SV30010, HyClone, USA). The plasmid transfection of MDA-MB-231 cells was carried out by following the manufacturer's protocol for Lipofectamine 2000 (11668019, Invitrogen, Carlsbad, CA, USA). The pcDNA3.1-LARP6 vector (NM_018357.4) was purchased from Youbio Biotech (Changsha, China). The cells transfected with the gene of interest were collected 48 h later for RT–qPCR and Western blot analysis.

MCF10A cells (CRL-10317, Shanghai Zhong Qiao Xin Zhou Biotechnology Co., Ltd., China) were cultured at 37 °C with 5% CO_2 in complete medium (ZQ-1311, Shanghai Zhong Qiao Xin Zhou Biotechnology Co., Ltd., China) containing 5% horse serum and 1% penicillin/streptomycin. MDA-MB-468, SUM159 and BT-20 cells were obtained from the Key Laboratory of Fertility Preservation, Ministry of Education. MDA-MB-468 cells were purchased from Wuhan Prosai Life Science Technology Co., Ltd. (CL-0290), SUM159 cells were purchased from Guangzhou Keluojie Biotechnology Co., Ltd. (KC0326), and BT-20 cells were purchased from Shanghai Zhongqiao Xinzhou Biotechnology Co., Ltd. (ZQ0940). We took appropriate measures to ensure that the quality of these cells was reliable, and we used these cells for our research to explore some of the characteristics of TNBC.

RNA extraction and RT-qPCR

Total RNA was isolated using TRIzol (Ambion). Afterwards, the RNA was subjected to chloroform extraction for further purification and then treated with RQ1 DNase (Promega, Madison, WI, USA) to eliminate any remaining DNA (if protein contamination was present, it was further purified via phenol–chloroform isoamyl alcohol). The quantity and quality of the purified RNA were assessed by measuring the absorbance at 260 nm/280 nm (A260/A280) on a Nanodrop One (Thermo). Additionally, the integrity of the RNA was confirmed via 1.0% agarose gel electrophoresis. The effects of LARP6 overexpression were assessed via the use of glyceraldehyde-3-phosphate dehydrogenase (GAPDH) as a control gene. cDNA synthesis was performed via standard procedures, and RT-qPCR analysis was carried out on a Bio-Rad S1000 instrument with HieffÔ qPCR SYBR® Green Master Mix (Low Rox Plus; YEASEN, China). The concentration of each transcript was subsequently normalized to the level of GAPDH mRNA via the $2^{-\Delta\Delta CT}$ method. The RT–qPCR sequences of primers used were as follows: LARP6 forward sequence: 5′-CCGCAAGTGTATGGATTATTC-3′, reverse sequence: 5′-CTCTGGTGTTGTC AGGAC-3′; GAPDH forward sequence: 5′-GGTCGGAGTCAACGGATTTG-3′, reverse sequence: 5′-GGAAG ATGGTGATGGGATTTC-3′. The primer sequences for the other genes are shown in the Supplementary Data.

Western blotting

MDA-MB-231 cells were lysed in ice-cold RIPA buffer (PR20001, Proteintech, China) supplemented with a protease inhibitor cocktail (4693116001, Sigma, USA) and incubated on ice for 30 min. The samples were boiled for 10 min in boiling water with protein loading buffer (P1040, Solarbio, China) and loaded onto a 10% SDS–PAGE gel, and RNA-binding proteins were transferred onto 0.45 mm PVDF membranes (ISEQ00010, Millipore, USA). The PVDF membranes were then blocked for 1 h at room temperature and incubated overnight at 4 °C with primary antibodies against FLAG tag (anti-FLAG, 1:2000, antibody produced in rabbit, 66008-3-Ig, ABclonal) and GAPDH (1:1000, antibody produced in rabbit, 60004-1-IG, Proteintech), followed by incubation with horseradish peroxidase-conjugated secondary antibodies (anti-rabbit, 1:5000, SA00001-2, Proteintech, China or anti-mouse, 1:5000, AS003, ABclonal, China) for 45 min at room temperature. Then, the membranes were visualized via chemiluminescence with enhanced ECL reagent (P0018FM, Beyotime, China). The LARP6 primary antibody used for the MCF10A and TNBC cells was an IgG antibody (1:2000, antibody produced in rabbits, 383B8A17) purchased from Thermo Fisher Scientific, and the β-actin antibody (1:5000, antibody produced in rabbits, 221050321) was purchased from Proteintech.

Cell proliferation assay

The Cell Counting Kit-8 (CCK-8, 40203ES76, Yeasen, Shanghai, China) assay was used to conduct the cell proliferation assay. In brief, MDA-MB-231 cells were plated at a density of 10,000 cells/well in 96-well culture plates. The cells in both the control group and the experimental group were treated appropriately, and vials without cells were used as blank controls. Following culture for 0, 24, 48 and 72 h at 37 °C and 5% CO_2, 10 μl of CCK-8 solution was added to the culture medium and incubated for an additional 3 h at 37 °C. The optical density of the cells was subsequently measured with a microplate reader (ELX800, Biotek, USA) at an absorbance of 450 nm. To calculate the cell proliferation rate, the following formula was used: proliferation rate = (experimental OD value – blank OD value)/(control OD value – blank OD value) × 100%.

Cell invasion assay

Transwell chambers (3422, Corning, USA) were utilized for conducting in vitro invasion assays. Transwell chambers with 8 μm filters precoated with a thin layer of Matrigel (356234, BD Biosciences, USA) were diluted 1:8 with serum-free medium, and 100 μl of diluted Matrigel in each chamber was incubated for 1 h at 37 °C and 5% CO_2, after which the unsolidified supernatant was removed. A total of 5×10^5 cells in 0.2 ml of serum-free medium were added to the inserts, after which the Transwell chambers were inserted in medium supplemented with 600 μl of 10% FBS (10091148, Gibco, China), which served as a chemoattractant in the lower chamber, and incubated for 48 h at 37 °C and 5% CO_2. Afterwards, the cells remaining on the upper membrane surface of the inserts were removed using a cotton swab. The total number of cells that penetrated the lower chamber were then fixed with 4% paraformaldehyde (P0099; Beyotime, China) for 20 min and subsequently stained with 0.1% crystal violet (C0121; Beyotime, China). The invading cells were observed and counted under an inverted microscope (MF52-N, Mshot, China) at 200× magnification.

RNA sequencing (RNA-seq)

The RNA extraction method remained unchanged. The KCTM Stranded mRNA Library Prep Kit for Illumina (Catalogue No. DR08402, Wuhan Seqhealth Co., Ltd., China) was used to construct a stranded RNA-seq library. According to the manufacturer's instructions, a total of 2 μg of total RNA was used for RNA library construction through the steps of mRNA enrichment, mRNA fragmentation, reverse transcription, adapter ligation, and PCR amplification. The concentration of the library was measured using a Qubit 4.0. The PCR products within the range of 200–500 base pairs were enriched and quantified. Finally, sequencing was performed on a NovaSeq 6000 sequencer (Illumina) in PE150 mode.

RNA-Seq Raw data cleaning and alignment

First, raw reads containing more than 2-N bases were discarded. Next, adaptors and low-quality bases were removed from the raw sequencing reads via FASTX-Toolkit (version 0.0.13). Additionally, short reads less than 16 nt in length were dropped. The clean reads were subsequently aligned to the GRCh38 genome using HISAT2[12], allowing 4 mismatches. Only uniquely mapped reads were used for gene read counting and FPKM (fragments per kilobase of transcript per million fragments mapped reads) calculation[13].

Differentially expressed genes (DEGs) analysis

The DESeq2[14] R Bioconductor package was used to identify DEGs. DEGs were identified on the basis of the cut-off criteria of an FDR-adjusted p value < 0.05 and an original fold change > 1.5 or < 2/3.

Alternative splicing analysis

The ABLas pipeline was used to define and quantify alternative splicing events (ASEs) and regulated alternative splicing events (RASEs) between the samples, as described in the previous section, where RNA-binding proteins connect in the future[15]. ABLas detected ten types of ASEs on the basis of splice junction reads, which included exon skipping (ES), alternative 5′ splice site (A5SS), alternative 3′ splice site (A3SS), mutually exclusive exons (MXE), mutually exclusive 5′ UTRs (5pMXE), mutually exclusive 3′ UTRs (3pMXE), cassette exons, A3SS&ES, and A5SS&ES.

To evaluate the significance of the ratio alteration of ASEs and determine RBP-regulated ASEs, a Student's t test was conducted. ASEs that demonstrated significance at a P value cut-off corresponding to a 5% false discovery rate were considered RBP-regulated ASEs.

Functional enrichment analysis

To identify functional categories of DEGs and peak-associated genes (target genes), we utilized the KOBAS 2.0 server[16] for GO term and KEGG pathway enrichment analyses. The enrichment of each term was defined via the hypergeometric test and the Benjamini–Hochberg false discovery rate (FDR) controlling procedure.

iRIP-Seq: coimmunoprecipitation and library preparation

MDA-MB-231 cells were irradiated once 400 mJ/cm^2 and lysed in ice-cold wash buffer. Cell lysis was performed in cold wash buffer (1× PBS, 0.1% SDS, 0.5% NP-40 and 0.5% sodium deoxycholate) supplemented with 400 U/mL RNase inhibitor (Takara) and protease inhibitor cocktail (Bimake) and incubated on ice for 30 min. The clear cell lysate was centrifuged at 10,000 rpm for 10 min at 4 °C. To achieve a final concentration of 0.1 U/μl, RQ I (Promega, M6101) was added, and the mixture was incubated at 37 °C for 30 min in a heat block. After vigorous vibration, the mixture was centrifuged at 13,000 × g at 4 °C for 15 min to eliminate any cell debris. Then, RNA digestion by MNase (Takara, 2910 A) was performed, and 0.5 M EDTA was added to stop the digestion.

For immunoprecipitation, the supernatant was incubated overnight at 4 °C with 10 μg of anti-Flag antibody (Sigma–Aldrich: F7425) and control IgG-conjugated antibody (AC005). The immunoprecipitates were subsequently incubated with protein A/G Dynabeads (Thermo Scientific, 26162) for 2 h at 4 °C. After magnet application and supernatant removal, the beads were sequentially washed with lysis buffer, high-salt buffer (250 mM Tris 7.4, 750 mM NaCl, 10 mM EDTA, 0.1% SDS, 0.5% NP-40 and 0.5 deoxycholate), and PNK buffer (50 mM Tris, 20 mM EGTA and 0.5% NP-40) for two rounds each. The beads were resuspended in elution buffer, which was composed of 50 mM Tris 8.0, 10 mM EDTA and 1% SDS. The suspension was placed in a heat block at 70 °C for 30 min to release the immunoprecipitated RBP with crosslinked RNA. The mixture was vortexed, and then the magnetic beads were separated via a separator. The resulting supernatant was transferred to a clean 1.5 ml microfuge tube. Proteinase K (Sangon Biotech, B600169) was added to the 10% input mixture (without immunoprecipitation), and RBP was immunoprecipitated with crosslinked RNA at a final concentration of 1.2 mg/ml. The mixture was incubated for 120 min at 55 °C. The RNA was purified with phenol: chloroform:

isopentyl alcohol (25:24:1 pH < 5) reagent (Solarbio, p1011). cDNA libraries were prepared with the KAPA RNA Hyper Prep Kit (KAPA, KK8541) according to the manufacturer's procedure. The libraries were prepared according to the manufacturer's instructions for high-throughput sequencing and then subjected to 150 nt paired-end sequencing on the Illumina NovaSeq system 6000.

iRIP-seq data analysis

Sequence alignment was performed as previously indicated. Two software programs, Piranha (Version 1.2.1, Peak Identification and Motif Discovery for High—Throughput Sequencing Data, https://github.com/smithlabcode/piranha) and ABLIRC, were subsequently used to perform peak calling. Piranha has been described elsewhere[17]. ABLIRC was used to identify the binding regions as previously described[18]. The process of peak calling was as follows: first, the whole genome was scanned with 5 bp as a window and 5 bp as a step from the beginning of each chromosome. The peak was identified by requiring that the depth of the first window be 2.5 times greater for 8 consecutive windows on the genome or that the average depth of the first window be greater than 50. When 8 consecutive windows were less than 4% of the maximum depth of this peak, the peak ended. At the same time, the reads for each gene were randomly distributed to each gene 500 times, and the frequency of the peak depth of each peak was assessed to conduct a significance analysis on the identified peaks and screen out the peaks with a significant ($P < 0.05$) or maximum depth of a certain degree (≥ 10). Then, with the input samples as the control, abundance difference analysis was conducted for the locations of these peaks, and the peak with an IP abundance greater than 4 times (adjustable parameter) the input abundance was screened as the final binding peak. The target genes of IP were ultimately determined by the peaks, and the binding motifs of the IP protein were identified via HOMER (Hypergeometric Optimization of Motif EnRichment, http://homer.ucsd.edu/homer/) software[19].

Data availability

The data discussed in this publication can be accessed with the GEO series accession number GSE248132.

Results

LARP6 is significantly upregulated in TNBC cell lines compared to normal breast cells

First, Western blotting was conducted to assess the expression level of LARP6 in both normal breast cells and TNBC cells. The findings revealed significantly greater expression of LARP6 in TNBC cells than in normal breast cells ($P < 0.05$) (Fig. 1).

LARP6 overexpression influences the proliferation and invasion of MDA-MB-231 cells

We subsequently created a cell model in which LARP6 was overexpressed in MDA-MB-231 cells. The LARP6-overexpressing (OE-LARP6) and negative control (NC) cell groups were constructed via plasmid transfection, and the expression level of LARP6 was detected by RT-qPCR (Fig. 2A) and Western blotting (Fig. 2B). Next, we explored whether LARP6 overexpression affects the proliferation and invasion of MDA-MB-231 cells via CCK-8 and Transwell assays. CCK-8 assays revealed that the survival rate of the OE-LARP6 group was significantly greater than that of the NC group at 72 h ($P < 0.05$) (Fig. 2C). Transwell assays revealed that the number of cells stained with crystal violet in the OE-LARP6 group was significantly greater than that in the NC group ($P < 0.0001$) (Fig. 2D).

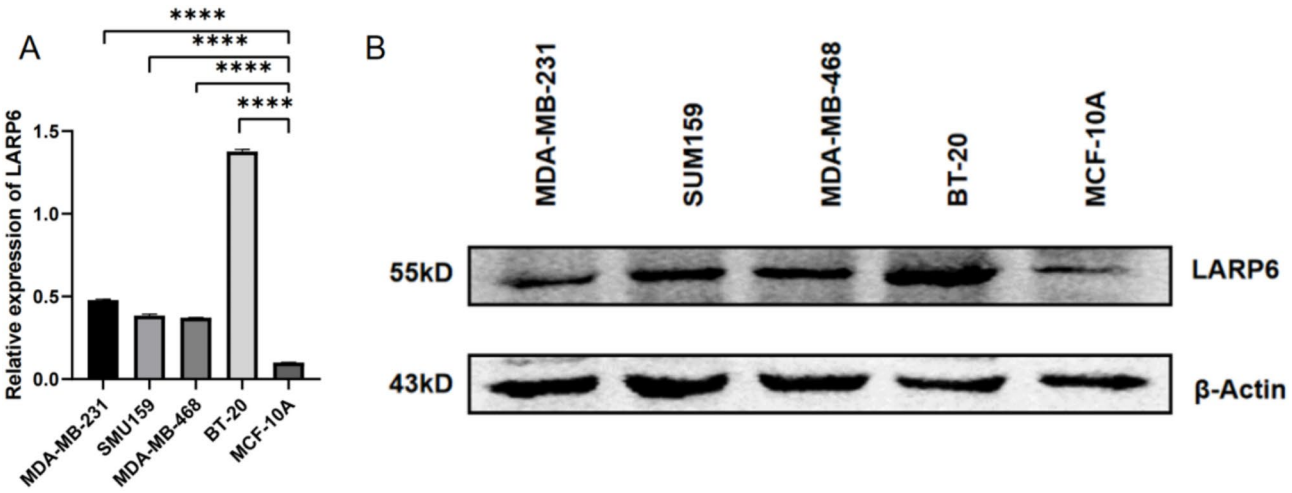

Fig. 1. LARP6 is highly expressed in TNBC cell lines. (**A**) Bar graph of the Western blotting results (MDA-MB-231, SMU159, MDA-MB-468 and BT-20 are TNBC cell lines, and MCF-10 A is a normal breast cell line). (**B**) Western blot band map. ****$P < 0.00001$.

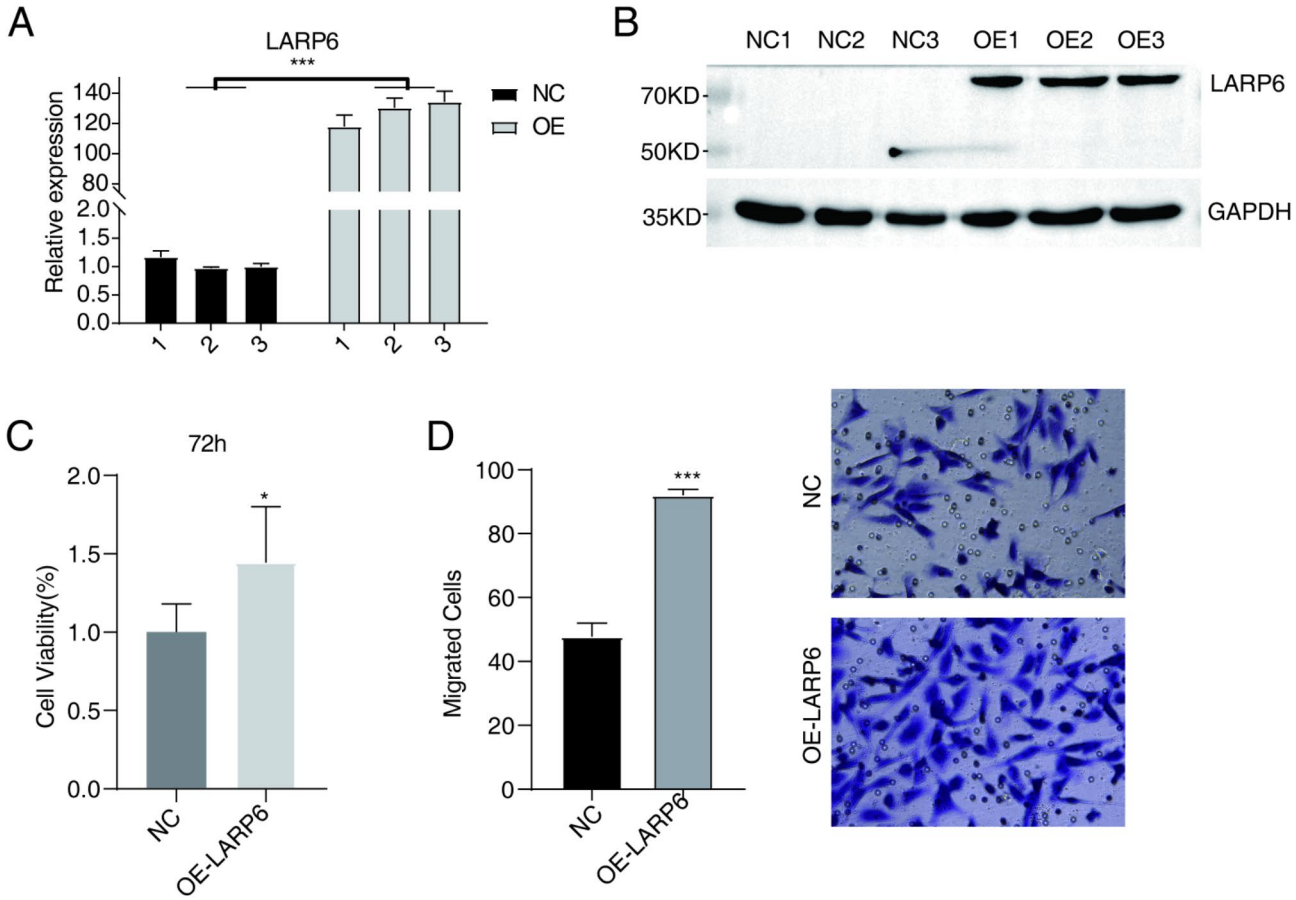

Fig. 2. LARP6 overexpression promotes the proliferation and invasion of MDA-MB-231 cells. (**A**) The histogram shows the RT-qPCR results for the control and treatment samples. The error bars represent the means ± SEMs. *$P < 0.05$, *** P value < 0.001. (**B**) Western blot analysis revealed that LARP6 overexpression was successful. (**C**) Proliferation assay results sfor MDA-MB-231 cells after LARP6 overexpression. (**D**) Cell invasion results for MDA-MB-231 cells after LARP6 overexpression.

LARP6 regulates the transcriptome in MDA-MB-231 cells

We carried out RNA-seq on cells from the OE-LARP6 group and NC group to examine alterations in the gene expression profile of MDA-MB-231 cells following LARP6 overexpression. Figure 3A shows that LARP6 was highly expressed in the OE-LARP6 group at the transcriptional level. Principal component analysis (PCA) revealed that the NC group and the OE-LARP6 group could be well distinguished, indicating that the two groups were comparable (Fig. 3B). A comparison of the gene expression of the two groups revealed that the number of DEGs reached 171 (105 were upregulated and 66 were downregulated), which indicated that LARP6 overexpression affects the expression of some genes in MDA-MB-231 cells (Fig. 3C). The genes in the NC group and OE-LARP6 group were analysed 3 times, and the expression of all the genes detected in each sample was analysed via sample cluster analysis (Fig. 3D). The experimental results demonstrated excellent repeatability. We performed GO enrichment analysis on the downregulated genes to elucidate their functions, and the results indicated their predominant involvement in the immune response (Fig. 3E). Then, according to the P value, we selected 8 DEGs for RT-qPCR verification and found that their expression levels were consistent with those identified by RNA-seq (Fig. 3F). These genes might have tumour-promoting or tumour-suppressing functions in TNBC.

LARP6 influences the AS of genes in MDA-MB-231 cells

The RNA-seq data were also used to assess AS. A comparison of the ASEs of the OE-LARP6 group and the NC group revealed that the number of regulated alternative splicing genes (RASGs) reached 1575 (796 upregulated AS events and 779 downregulated AS events) (Table 1), indicating that LARP6 overexpression can affect the AS of many genes in MDA-MB-231 cells.

Through the analysis of AS, we found that LARP6 overexpression affected multiple ASEs in MDA-MB-231 cells (Fig. 4A). Similarly, a clustering heatmap was generated for three replicate samples from the NC group and the OE-LARP6 group, and the consistency of the two groups of samples was good (Fig. 4B). Next, we conducted GO enrichment analysis of the RASGs, and the results revealed that 4 of the top 10 significantly enriched pathways were related to DNA replication and repair (Fig. 4C). Finally, to determine the accuracy of

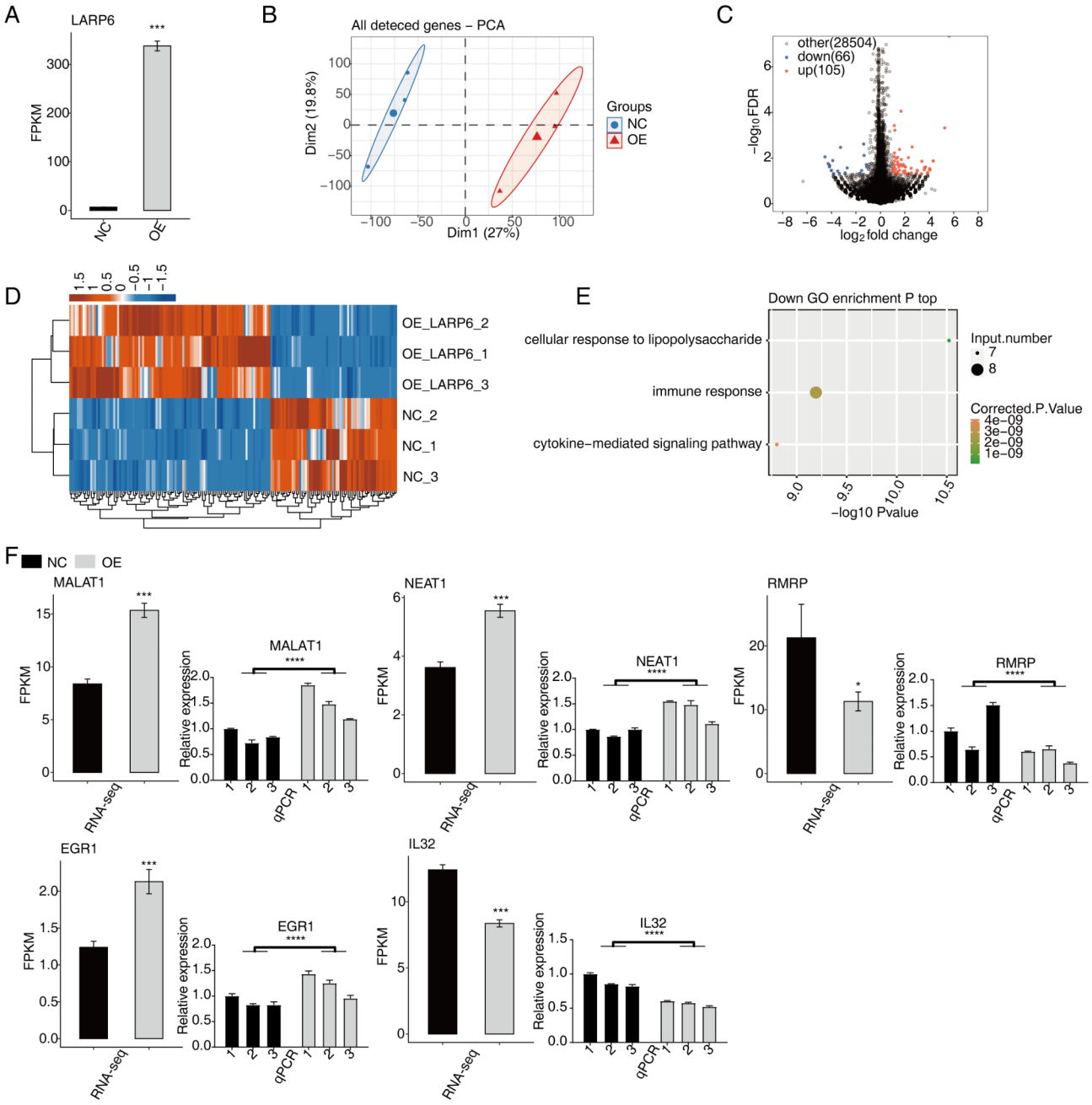

Fig. 3. LARP6 overexpression affects the expression of genes in MDA-MB-231 cells. (**A**) Bar plot showing the expression patterns and significant differences in DEGs related to LARP6. The error bars represent the means ± SEMs. ***P value < 0.001. (**B**) PCA of the FPKM values of all the genes detected after LARP6 overexpression. The ellipse for each group indicates the confidence interval. (**C**) Volcano plot showing all DEGs between the OE and NC samples. (**D**) Hierarchical clustering heatmap showing the expression levels of all DEGs. (**E**) Bubble plot showing the top 3 enriched GO biological process results of the downregulated DEGs. (**F**) Bar plot showing the expression patterns and significant differences in DEGs among some important genes. The error bars represent the means ± SEMs. ***P value < 0.001, **P value < 0.01, *P value < 0.05.

AS analysis, we selected the genes encoding RASG WW and C2 domain-containing protein 1 (WWC1) and SLC9A3R2. We then verified the changes in AS in the OE-LARP6 group and the NC group via RT-qPCR. The AS patterns were quantified by calculating the inclusion/exclusion (In/Ex) ratios. AS analysis revealed that the overexpression of LARP6 upregulated the A3SS of WWC1 and the A5SS of SLC9A3R2, which was consistent with the results verified by RT-qPCR (Fig. 4D).

Sample	Type	3pMXE	5pMXE	A3SS	A3SS&ES	A5SS	A5SS&ES	ES	MXE	Cassetteexon	Total
OE-LARP6 vs. NC	Up	60	50	184	28	195	27	116	32	104	796
OE-LARP6 vs. NC	Down	62	57	188	28	160	29	104	54	97	779

Table 1. Statistics of RASEs. *ES, exon skipping; A5SS, alternative 5'splice site; A3SS, alternative 3'splice site; MXE, mutually exclusive exons; 5pMXE, mutually exclusive 5'UTRs; 3pMXE, mutually exclusive 3'UTRs.

iRIP-seq of LARP6 in MDA-MB-231 cells

Through iRIP-seq, we analysed the binding profile of LARP6 in MDA-MB-231 cells. First, the binding specificity of the LARP6 antibody and the effectiveness of the immunoprecipitation technique were confirmed by Western blotting, and two groups (IP-1 and IP-2) of repeated experiments were set up (Fig. 5A). We found that LARP6 binds to the 5′ untranslated region (5′′UTR), 3′ untranslated region (3′UTR), coding sequence (CDS), Nc_exon, introns, intergenic region, and antisense region of RNA (Fig. 5B). The CDS was the most common binding site (Fig. 5C). The motif of the LARP6 binding peak was subsequently analysed via HOMER software, and the first five binding motifs in two repeated IP samples were obtained. The binding motifs of the two groups had CGACGAG sequences, and those of the other groups were also similar (Fig. 5D). Second, we intersected the binding peaks of the two groups and found 312 overlapping binding peaks (Fig. 5E). Finally, we performed GO enrichment analysis on the genes with overlapping binding peaks and found that they were enriched in multiple pathways related to transcription and translation regulation. Moreover, the genes were enriched in the negative regulation of the apoptosis process, cell proliferation, cell motility and other pathways (Fig. 5F). These findings indicate that LARP6 performs posttranscriptional regulation by recognizing and combining with the unique sequence of RNA.

Integrated analysis of transcriptome data and iRIP-Seq

Through gene annotation and correlation analysis of binding peak reads, we found that there were 255 binding peak-related genes. We then intersected these genes with the DEGs of the transcriptome and obtained the differentially expressed binding peak-related genes (LARP6 and EGR1) (Fig. 6A). Interestingly, we found that LARP6 can interact with its own RNA. We further studied the binding site between LARP6 and its own RNA. The location of this site in the genome is shown in Fig. 6B. Finally, our iRIP–PCR validation of LARP6 binding to self-RNA revealed that LARP6 was significantly enriched in LARP6 immunoprecipitates compared with the input control.

Integration analysis of AS and iRIP-seq

To further investigate the genes by which LARP6 binds to and regulates AS, we performed an overlap analysis of RASGs enriched in the RNA-seq dataset and peak genes identified via iRIP-seq, which revealed 16 overlapping genes (PTPN11, PTMS, LARP6, SLC9A3R2, NT5C3B, DAZAP1, TCEA2, NSD2, FLOT1, TMUB1, YWHAZ, CYHR1, RDX, RPL27a, RNF126, and MZT2B) (Fig. 7A). KEGG enrichment analysis was performed on these overlapping genes, and the main enriched term was proteoglycans in cancer (Fig. 7B). Among these genes, we noted PTMS, SLC9A3R2, and TMUB1, whose dysregulation is associated with cell proliferation and drug resistance[20–22].

In this study, iRIP-seq revealed that LARP6 overexpression promoted A3SS events for PTMS and A5SS events for SLC9A3R2 and suppressed A3SS events for LARP6, which was consistent with the results of our validation experiment involving iRIP-PCR (Fig. 7C). Next, we investigated the binding sites between LARP6 and PTMS in the genome, as shown in Fig. 7D. Finally, iRIP–PCR validation revealed that compared with the input control, PTMS was significantly enriched in LARP6 immunoprecipitates. We explored the binding sites between TMUB1 and LARP6 in the same way, and the iRIP-PCR results revealed that TMUB1 was enriched in LARP6 immunoprecipitates (Fig. 7E).

Discussion

Previous studies have shown that posttranscriptional regulation of RBP expression plays a crucial role in regulating the occurrence and progression of TNBC[23]. Further research and a better understanding of the function of RBPs in TNBC may help to identify biomarkers that can predict patient prognosis and therapeutic effects and to evaluate potential new targets to develop new treatments for TNBC. In our study, we clarified the mechanism by which LARP6 functions as an RBP in TNBC.

LARP6 plays a cancer-promoting role in most cancer diseases[10,11]. In this study, we found that LARP6 expression is upregulated in TNBC cell lines and promotes the proliferation and invasion of MDA-MB-231 cells. Our findings align with the results reported by Shao R et al.[24]. According to the RNA-seq transcriptome data, LARP6 overexpression affects the expression levels of 171 genes, and according to the iRIP-seq results, only 2 genes are directly regulated by LARP6. These findings suggest that LARP6 is not a significant factor in regulating gene expression. In contrast, the AS analysis results indicated that LARP6 affects almost all types of ASEs, mainly A3SS and A5SS events. It has been reported that genes with differential A3SS splicing are enriched in splicing and RNA processing gene sets[25]. This finding shows that a better understanding of the regulatory role of alternative splice sites is very valuable. The regulation of splice site usage is important for selective pre-mRNA splicing to correctly express protein isoforms in cells, but its disruption can lead to diseases, including cancer[26,27]. For example, a mutation from AA to AG creates a hidden 3' splice site that adds 11 nucleotides to BRCA1 mRNA, which encodes a truncated protein in the breast cancer family[28]. Moreover, compared with the

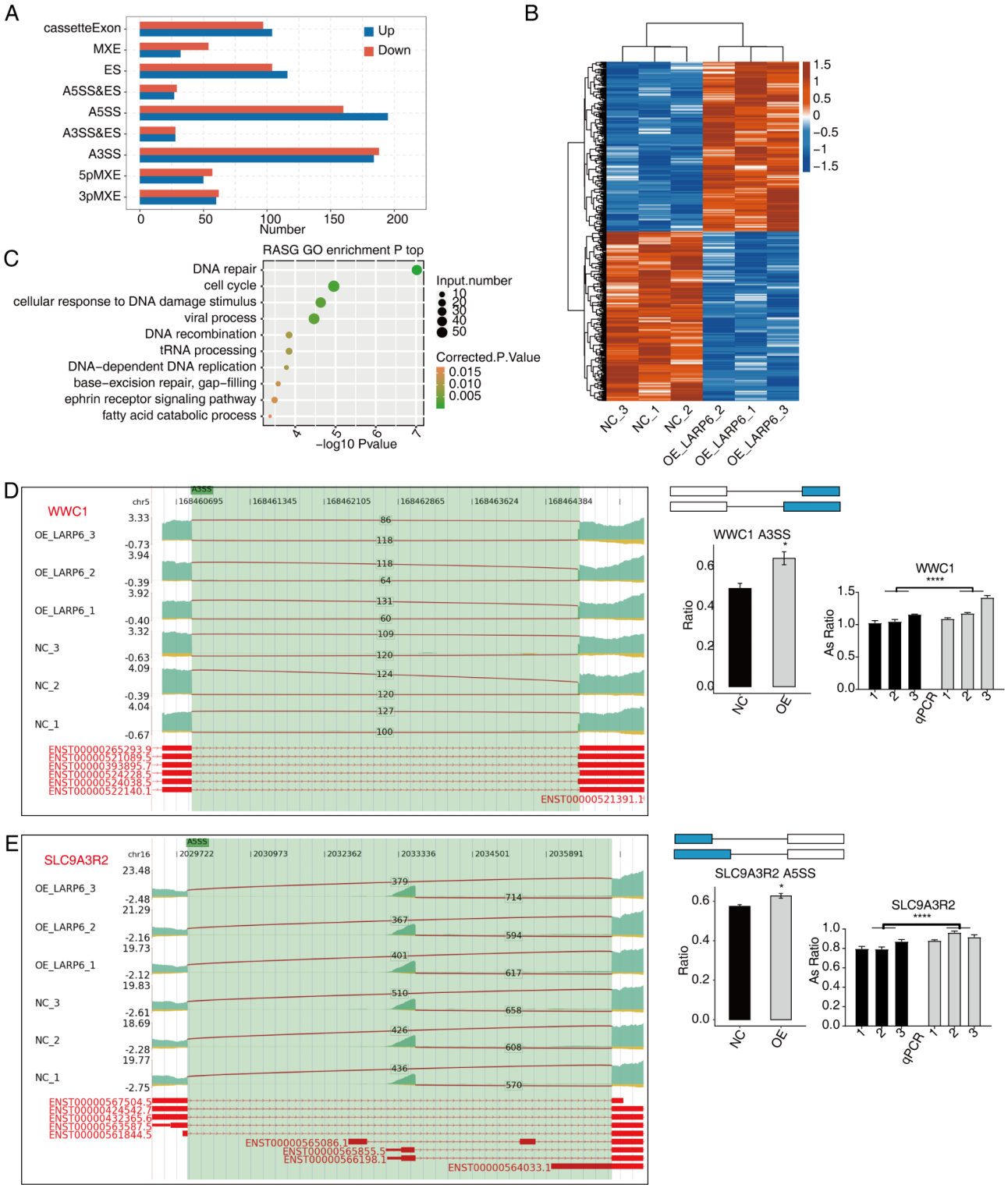

Fig. 4. LARP6 influences the AS of genes in MDA-MB-231 cells. (**A**) Bar plot showing the LARP6 RASEs. (**B**) Hierarchical clustering heatmap based on AS ratio values. (**C**) Scatter plot showing the top 10 enriched GO biological process results of the RASGs. (**D**) LARP6 regulates alternative splicing of WWC1 and SLC9A3R2. Left panel: IGV-Sashimi plot showing the RASEs and binding sites across mRNAs. The read distribution of RASE is plotted in the upper panel, and the transcripts of each gene are shown below. Right panel: Schematic diagrams depicting the structures of A3SS and A5SS. The results of RNA-seq validation of the A3SS and A5SS are shown at the bottom of the right panel. The error bars represent the means ± SEMs. *P value < 0.05. ****P value < 0.0001.

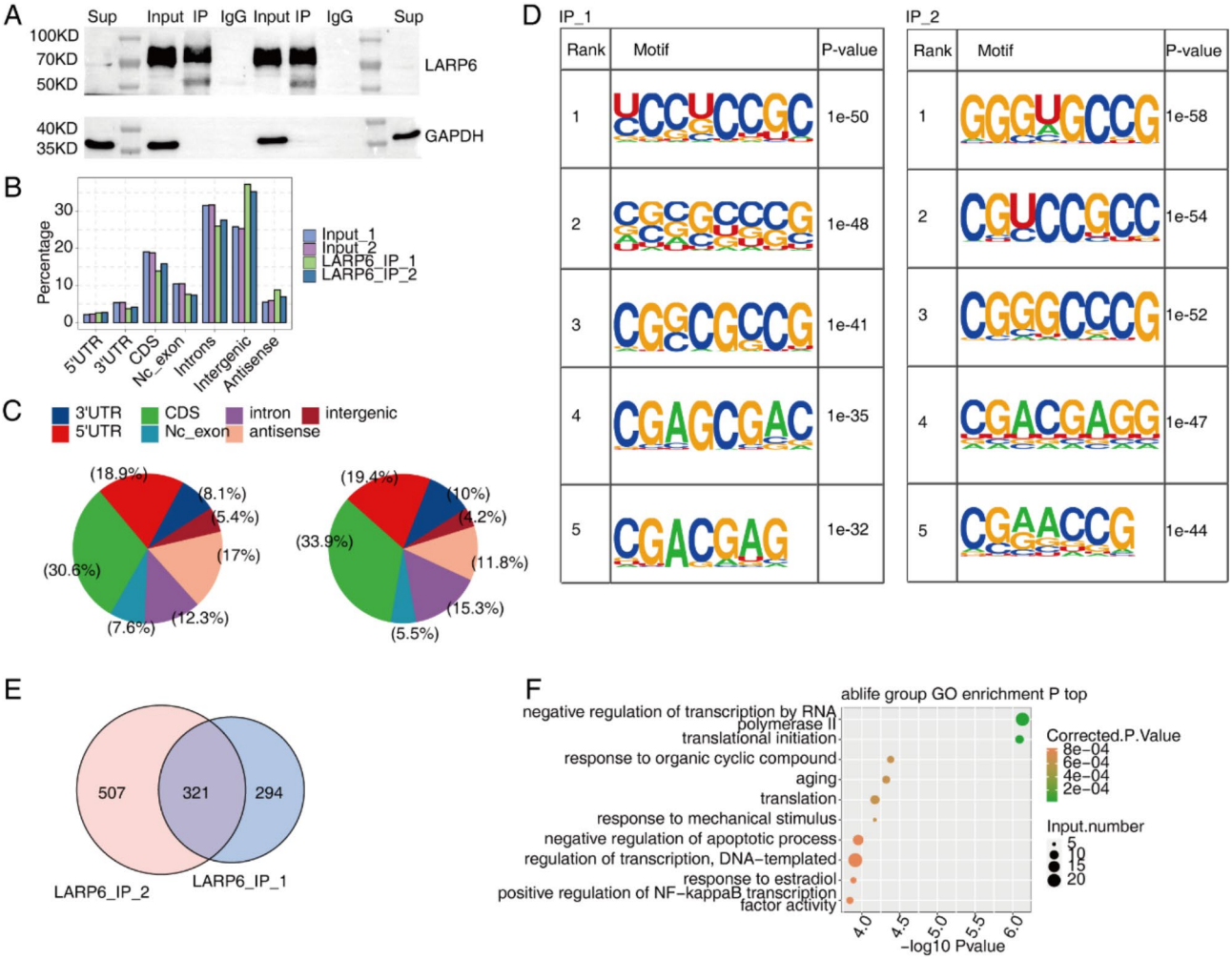

Fig. 5. RNA binding profile of LARP6 in MDA-MB-231 cells. (**A**) Western blotting of LARP6 immunoprecipitates with an anti-Flag monoclonal antibody; two replicates were performed (The WB band of GAPDH appears to have the membrane edges too close due to the light adjustment of the figure. The original figure can be viewed in the supplementary materials). (**B**) Bar plots showing the distribution of LARP6 iRIP-seq samples across different regions of the genome. (**C**) Pie chart showing the genomic distribution of LARP6-bound peaks from the two biological replicates. (**D**) Motif analysis results showing the enriched motifs from LARP6-bound peaks from the two biological replicates. (**E**) Venn diagram showing the overlapping binding peaks between two replicates. (**F**) Bubble plot showing the most enriched GO biological process results for the overlapping binding peaks.

number of DEGs, the number of differential RASGs was significantly greater. Therefore, LARP6 may play a cancer-promoting role by regulating gene splicing events.

When the DEGs and iRIP-seq results were combined, LARP6 was found to directly bind and affect the AS of 16 genes (PTPN11, PTMS, LARP6, SLC9A3R2, NT5C3B, DAZAP1, TCEA2, NSD2, FLOT1, TMUB1, YWHAZ, CYHR1, RDX, RPL27a, RNF126, and MZ2B). Among them, the protein tyrosine phosphatase SHP2 encoded by the proto-oncogene PTPN11 regulates the stability of cyclin D1 through the PI3K/AKT/GSK3β signalling pathway and increases the carcinogenic activity of β-catenin, thus promoting the proliferation and invasion of TNBC[29,30]. NSD2 is related to cell division, mitotic nuclear division and the transition of the mitotic cell cycle, and its overexpression can significantly promote the proliferation, migration and invasion of TNBC cells[31]. RPL27A is a ribosomal protein-encoding gene that is significantly upregulated in TNBC; it activates the EIF2 signalling pathway and promotes cancer cell invasion[32]. YWHAZ promotes the proliferation and invasion of cancer cells by inhibiting mitochondrial apoptosis, inducing anchoring-independent growth, malignant transformation of cancer cells and antiapoptotic effects[33]. TMUB1 is a ubiquitin-like protein that shuttles between the cytoplasm and nucleus. Many studies have shown that TMUB1 not only controls proliferation but also plays important roles in apoptosis, cycle regulation and genomic stability[34]. Therefore, we speculate that LARP6 can play a cancer-promoting role by affecting the AS of genes.

In addition, according to the GO enrichment analysis, RASGs were enriched in the important pathways of DNA repair, the cell response to DNA damage and the cell cycle. By using RT-qPCR, we verified that LARP6

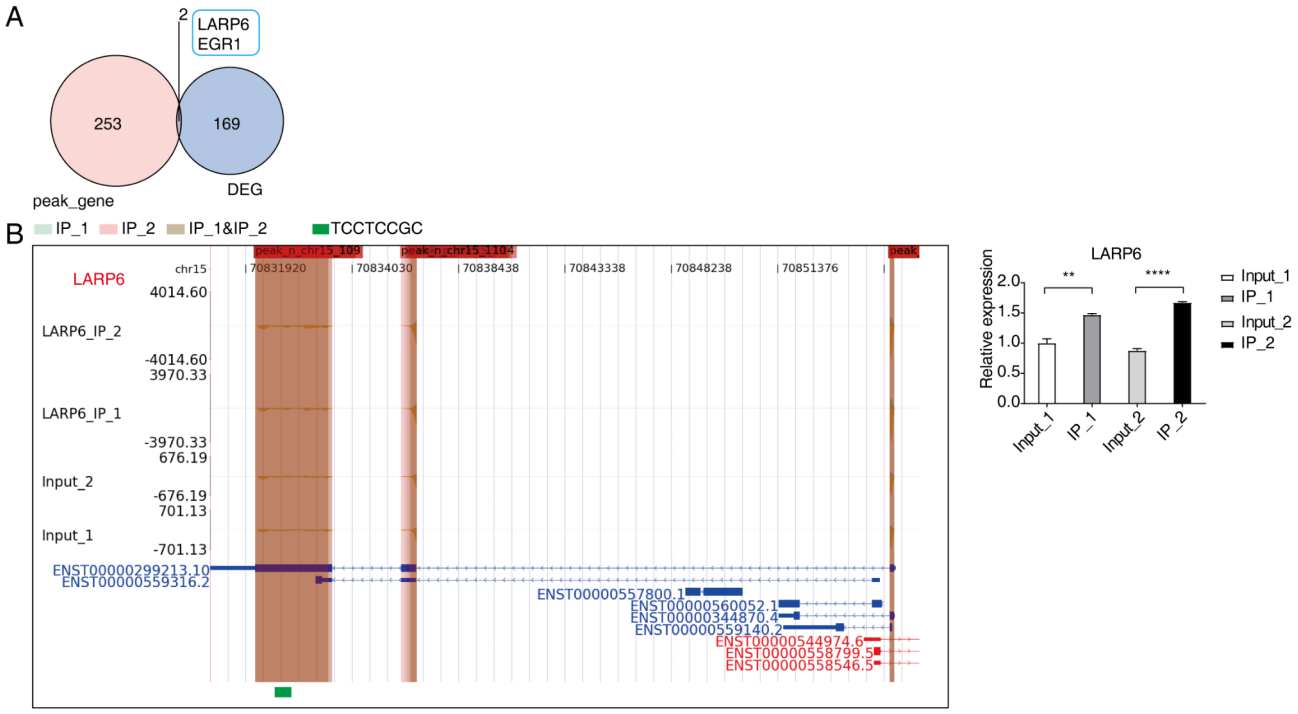

Fig. 6. LARP6 binds and regulates the expression of its own genes in MDA-MB-231 cells. (**A**) Venn diagram showing the overlapping genes between peak genes and DEGs. (**B**) LARP6 binding peak genes of LARP6. IGV-Sashimi plot showing the peak reads and binding sites across mRNAs; the green and red panels represent the positions of the peaks. The read distribution of the bound genes is plotted in the upper panel, and the transcripts of each gene are shown below. The panel on the right shows the validation results of RIP-PCR for LARP6. **P value < 0.01. ****P value < 0.0001.

overexpression increased the A3SS splicing level of WWC1. WWC1, also known as KIBRA, phosphorylates KIBRA to mediate the proliferation and migration of MDA-MB-231 cells, and it may also act as a scaffold protein or linker protein, which helps the platform to further recruit other DNA damage response factors, thus promoting DNA repair[35,36]. Most importantly, core anticancer therapy attempts to eradicate malignant cells by inducing DNA damage with ionizing radiation or chemicals[37,38]. Although there is a lack of direct evidence supporting the contribution of specific splicing variants involved in the DNA damage response (DDR) to the development of drug resistance, splicing-based regulation is prominent in the DDR pathway and may affect therapeutic drug resistance[39]. Studies have shown that after DNA double-strand break induction, BRCA1 recruits proteins involved in DNA repair at the damaged site and interacts with the RBPs BCLAF1 and THRAP3 to form complexes, thus regulating the expression of DDR genes through AS[39]. In some cancers, the main component of the DNA damage repair pathway is AS[40]. Therefore, we speculate that the inhibition of LARP6 may increase the sensitivity of TNBC cells to anticancer drugs.

In this study, we used iRIP-seq to elucidate the direct interaction between LARP6 and RNA in TNBC MDA-MB-231 cells. The results revealed that a significant portion of the LARP6 binding peaks were enriched in the CDS and 5' UTR regions. Furthermore, we identified the consensus sequence of LARP6-binding genes through motif analysis. Its binding sites on different genes are not the same, but there are certain commonalities. Our study reveals a CGACGAG binding motif, which provides a new perspective for further exploration of the cancer-promoting mechanism of LARP6 in tumour cells and may lead to the identification of new potential therapeutic targets. Interestingly, in this study, the LARP6 protein directly binds to its own RNA, reducing the occurrence of self-A3SS splicing events and altering the level of LARP6 mRNA expression. These findings provide directions for subsequent in-depth research.

The advantages of this study include the following: LARP6 enhances the growth and blood vessel formation of human breast cancer patients, and this activity depends on its nuclear localization[41]; however, the specific mechanism of action is unclear. Our study identified the target genes and binding motifs bound by LARP6 through RNA-seq and iRIP-seq high-throughput sequencing technologies, laying a solid foundation for continued research on the mechanism of action of LARP6 in TNBC. The limitations of this study are as follows: (1) No in vivo experiments have been conducted to verify the malignant biological behaviour of LARP6 in promoting TNBC. (2) The target genes of LARP6 have not been further verified at the molecular level.

Conclusion

Although we determined that LARP6 directly regulates the AS of TNBC-promoting genes, the exact mechanism by which LARP6 regulates the AS of related genes has not been fully elucidated, and further research is needed.

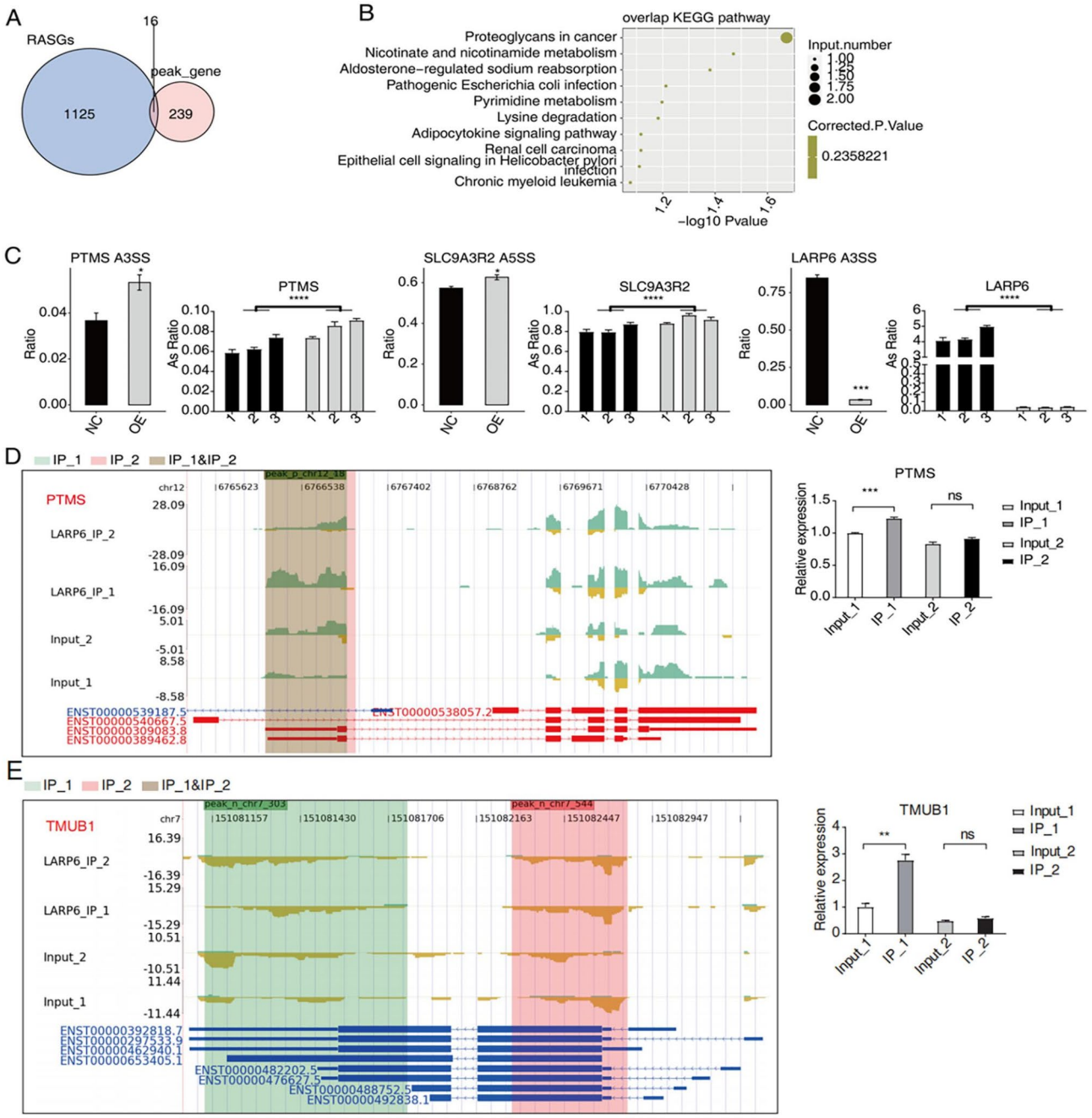

Fig. 7. LARP6 binds and regulates the AS of genes associated with proliferation and drug resistance in MDA-MB-231 cells. (**A**) Venn diagram showing the overlapping genes between peak genes and RASGs. (**B**) Scatter plot showing the most enriched KEGG pathway results for the overlapping genes. (**C**) Bar plot showing the ratio values for AS of some overlapping genes. The error bars represent the means ± SEMs. ****P value < 0.0001, ***P value < 0.001, *P value < 0.05. (**D**) LARP6 binding peak reads for PTMS. IGV-Sashimi plot showing the peak reads and binding sites across mRNAs; the green and red panels represent the positions of the peaks. The read distribution of the bound genes is plotted in the upper panel, and the transcripts of each gene are shown below. The right figure shows the iRIP-PCR results for PTMS. (**E**) LARP6 binding peak genes of TMUB1. IGV-Sashimi plot showing the peak reads and binding sites across mRNAs; the green and red panels represent the positions of the peaks. The read distribution of the bound genes is plotted in the upper panel, and the transcripts of each gene are shown below. The right figure shows the iRIP-PCR results for TMUB1.

In summary, our study provides a basis for an in-depth understanding of the role of LARP6 in various biological processes and provides new clues for targeted therapy for TNBC.

Data availability

The datasets generated and analysed during the current study are available in the Gene Expression Omnibus (GEO) repository, [https://www.ncbi.nlm.nih.gov/geo/query/acc.cgi?&acc=GSE248132].

Received: 4 November 2024; Accepted: 27 February 2025
Published online: 06 March 2025

References

1. Goldhirsch, A. et al. Panel, personalizing the treatment of women with early breast cancer: highlights of the St Gallen international expert consensus on the primary therapy of early breast Cancer 2013. *Ann. Oncol.* **24** (9), 2206–2223 (2013).
2. Howard, F. M. & Olopade, O. I. Epidemiology of Triple-Negative breast cancer: A review. *Cancer J.* **27** (1), 8–16 (2021).
3. Yin, L., Duan, J. J., Bian, X. W. & Yu, S. C. Triple-negative breast cancer molecular subtyping and treatment progress. *Breast Cancer Res.* **22** (1), 61 (2020).
4. Chaudhary, L. N., Wilkinson, K. H. & Kong, A. Triple-negative breast cancer: who should receive neoadjuvant chemotherapy?? *Surg. Oncol. Clin. N Am.* **27** (1), 141–153 (2018).
5. Kumar, H. et al. A review of biological targets and therapeutic approaches in the management of triple-negative breast cancer. *J. Adv. Res.* (2023).
6. Ge, J. Y. et al. Acquired resistance to combined BET and CDK4/6 Inhibition in triple-negative breast cancer. *Nat. Commun.* **11** (1), 2350 (2020).
7. Dermit, M. et al. Subcellular mRNA localization regulates ribosome biogenesis in migrating cells. *Dev. Cell.* **55**(3), 298–313 e10 (2020).
8. Stavraka, C. & Blagden, S. The La-related proteins, a family with connections to cancer. *Biomolecules* **5** (4), 2701–2722 (2015).
9. Blackstock, C. D. et al. Insulin-like growth factor-1 increases synthesis of collagen type I via induction of the mRNA-binding protein LARP6 expression and binding to the 5' stem-loop of COL1a1 and COL1a2 mRNA. *J. Biol. Chem.* **289** (11), 7264–7274 (2014).
10. Dai, S. et al. Development and validation of RNA binding protein-applied prediction model for gastric cancer. *Aging (Albany NY).* **13** (4), 5539–5552 (2021).
11. Yang, L. et al. Written on behalf of the, development and validation of a prediction model for lung adenocarcinoma based on RNA-binding protein. *Ann. Transl. Med.* **9** (6), 474 (2021).
12. Kim, D., Langmead, B. & Salzberg, S. L. HISAT: a fast spliced aligner with low memory requirements. *Nat. Methods.* **12** (4), 357–360 (2015).
13. Trapnell, C. et al. Transcript assembly and quantification by RNA-Seq reveals unannotated transcripts and isoform switching during cell differentiation. *Nat. Biotechnol.* **28** (5), 511–515 (2010).
14. Love, M. I., Huber, W. & Anders, S. Moderated estimation of fold change and dispersion for RNA-seq data with DESeq2. *Genome Biol.* **15** (12), 550 (2014).
15. Jin, L. et al. Transcriptome analysis reveals the complexity of alternative splicing regulation in the fungus verticillium dahliae. *BMC Genom.* **18** (1), 130 (2017).
16. Xie, C. et al. KOBAS 2.0: a web server for annotation and identification of enriched pathways and diseases. *Nucleic Acids Res.* **39** (Web Server issue), W316–W322 (2011).
17. Uren, P. J. et al. Site identification in high-throughput RNA-protein interaction data. *Bioinformatics* **28** (23), 3013–3020 (2012).
18. Xia, H. et al. CELF1 preferentially binds to exon-intron boundary and regulates alternative splicing in HeLa cells. *Biochim. Biophys. Acta Gene Regul. Mech.* **1860** (9), 911–921 (2017).
19. Heinz, S. et al. Simple combinations of lineage-determining transcription factors prime cis-regulatory elements required for macrophage and B cell identities. *Mol. Cell.* **38** (4), 576–589 (2010).
20. Barron-Gallardo, C. A. et al. A gene expression signature in HER2 + breast cancer patients related to neoadjuvant chemotherapy resistance, overall survival, and disease-free survival. *Front. Genet.* **13**, 991706 (2022).
21. Shi, C. et al. Promoting anti-tumor immunity by targeting TMUB1 to modulate PD-L1 polyubiquitination and glycosylation. *Nat. Commun.* **13** (1), 6951 (2022).
22. Qin, H. et al. RNA-binding proteins in tumor progression. *J. Hematol. Oncol.* **13** (1), 90 (2020).
23. Miles, W. O. et al. Alternative polyadenylation in Triple-Negative breast tumors allows NRAS and c-JUN to bypass PUMILIO posttranscriptional regulation. *Cancer Res.* **76** (24), 7231–7241 (2016).
24. Siegfried, Z. & Karni, R. The role of alternative splicing in cancer drug resistance. *Curr. Opin. Genet. Dev.* **48**, 16–21 (2018).
25. Levesque, L. A., Roy, S. & Salazar, N. CXCR3 expression and genome-wide 3' splice site selection in the TCGA breast cancer cohort. *Life (Basel, Switzerland)* **11**(8) (2021).
26. Sohail, M. & Xie, J. Diverse regulation of 3' splice site usage. *Cell. Mol. Life Sci.* **72** (24), 4771–4793 (2015).
27. Dybkov, O. et al. Regulation of 3' splice site selection after step 1 of splicing by spliceosomal C* proteins. *Sci. Adv.* **9** (9), eadf1785 (2023).
28. Tazi, J., Bakkour, N. & Stamm, S. Alternative splicing and disease. *Biochim. Biophys. Acta.* **1792** (1), 14–26 (2009).
29. Yuan, Y. et al. SHP2 promotes proliferation of breast cancer cells through regulating Cyclin D1 stability via the PI3K/AKT/GSK3beta signaling pathway. *Cancer Biol. Med.* **17** (3), 707–725 (2020).
30. Martin, E. & Agazie, Y. M. SHP2 potentiates the oncogenic activity of beta-Catenin to promote Triple-Negative breast Cancer. *Mol. Cancer Res.* **19** (11), 1946–1956 (2021).
31. Gao, B., Liu, X., Li, Z., Zhao, L. & Pan, Y. Overexpression of EZH2/NSD2 histone methyltransferase axis predicts poor prognosis and accelerates tumor progression in triple-negative breast cancer. *Front. Oncol.* **10**, 600514 (2020).
32. Zhao, W. et al. Ribosome proteins represented by RPL27A mark the development and metastasis of triple-negative breast cancer in mouse and human. *Front. Cell. Dev. Biol.* **9**, 716730 (2021).
33. Gan, Y., Ye, F. & He, X. X. The role of YWHAZ in cancer: A maze of opportunities and challenges. *J. Cancer.* **11** (8), 2252–2264 (2020).
34. Castelli, M. et al. Different functions of HOPS isoforms in the cell: HOPS shuttling isoform is determined by RIP cleavage system. *Cell cycle (Georgetown, Tex)* **13** (2), 293–302 (2014).
35. Yang, S. et al. Phosphorylation of KIBRA by the extracellular signal-regulated kinase (ERK)-ribosomal S6 kinase (RSK) cascade modulates cell proliferation and migration. *Cell. Signal.* **26** (2), 343–351 (2014).
36. Mavuluri, J. et al. Phosphorylation-dependent regulation of the DNA damage response of adaptor protein KIBRA in cancer cells. *Mol. Cell. Biol.* **36** (9), 1354–1365 (2016).
37. Cao, Q. et al. Macrophages as a potential tumor-microenvironment target for noninvasive imaging of early response to anticancer therapy. *Biomaterials* **152**, 63–76 (2018).

38. Sharma, A. et al. Hypoxia-targeted drug delivery. *Chem. Soc. Rev.* **48** (3), 771–813 (2019).
39. Vohhodina, J. et al. The RNA processing factors THRAP3 and BCLAF1 promote the DNA damage response through selective mRNA splicing and nuclear export. *Nucleic Acids Res.* **45** (22), 12816–12833 (2017).
40. Rahmutulla, B., Matsushita, K. & Nomura, F. Alternative splicing of DNA damage response genes and Gastrointestinal cancers. *World J. Gastroenterol.* **20** (46), 17305–17313 (2014).
41. Shao, R. et al. The novel lupus antigen related protein Acheron enhances the development of human breast cancer. *Int. J. Cancer.* **130** (3), 544–554 (2012).

Author contributions

J.L. developed the overall research goals and provided financial support. L.G. performed the cell experiments and wrote the first draft of the manuscript. Y. L. conducted the verification experiments and provided research materials. S.Y. collected experimental data. H.L. analyzed the experimental data and made figures. K.Z. reviewed and modified the manuscript. The final version of the manuscript was reviewed by all authors. The author(s) read and approved the final manuscript.

Funding

This work was supported by the Key Research and Development Program of Ningxia Hui Autonomous Region [grant number 2021BEG03062] and the Sixth Batch of Youth Science and Technology Lift Projects in the Ningxia Hui Autonomous Region (Yaobang Liu).

Declarations

Competing interests

The authors declare no competing interests.

Ethical approval

This study did not involve animal experiments or human subjects, and ethical consent and animal care standards were not needed.

Additional information

Supplementary Information The online version contains supplementary material available at https://doi.org/10.1038/s41598-025-92351-8.

Correspondence and requests for materials should be addressed to J.L.

Reprints and permissions information is available at www.nature.com/reprints.

Publisher's note Springer Nature remains neutral with regard to jurisdictional claims in published maps and institutional affiliations.